

Plan B: New Z' models for $b \rightarrow s\ell^+\ell^-$ anomalies

Ben Allanach^a and Anna Mullin^{b,1}

^a*DAMTP, University of Cambridge, Wilberforce Road, Cambridge, CB3 0WA, United Kingdom*

^b*Department of Physics, Cavendish Laboratory, JJ Thomson Avenue, Cambridge, CB3 0HE, United Kingdom*

E-mail: B.C.Allanach@damtp.cam.ac.uk, ajm351@cam.ac.uk

ABSTRACT: Measurements of $b \rightarrow s\mu^+\mu^-$ transitions indicate that there may be a new physics field coupling to di-muon pairs associated with the b to s flavour transition. Including the 2022 LHCb reanalysis of R_K and R_{K^*} , one infers that there may also be associated new physics in $b \rightarrow se^+e^-$ transitions. Here, we examine the extent of the statistical preference for Z' models coupling to di-electron pairs taking into account the relevant constraints, in particular from experiments at LEP-2. We identify an anomaly-free set of models which interpolates between the Z' not coupling to electrons at all, to one in which there is an equal Z' coupling to muons and electrons (but where in all models in the set, the Z' boson can mediate $b \rightarrow s\mu^+\mu^-$ transitions). A $3B_3 - L_e - 2L_\mu$ model provides a close-to-optimal fit to the pertinent measurements along the line of interpolation. We have (re-)calculated predictions for the relevant LEP-2 observables in terms of dimension-6 SMEFT operators and put them into the `flavio` computer program, so that they are available for global fits.

KEYWORDS: B -anomalies, beyond the Standard Model, flavour changing neutral currents

¹Corresponding author.

Contents

1	Introduction	1
2	SMEFT operator fit	3
2.1	Fit results	4
3	Models	6
3.1	Fermionic charge assignment	6
3.2	More model details	9
4	LEP constraints	13
4.1	LEP: di-muon and di-tau final states	13
4.2	LEP: Bhabha scattering	15
5	Fits	16
5.1	$3B_3 - L_e - 2L_\mu$	18
6	Conclusion	21

1 Introduction

Various measurements of B -meson decays at LHC experiments are in tension with Standard Model (SM) predictions, particularly when the final state includes a di-muon pair. For example the CMS, ATLAS and LHCb combined [1–3] CP-untagged, time integrated branching ratio of B_s decaying to di-muon pairs $\overline{BR}(B_s \rightarrow \mu^+ \mu^-)$ [1, 3, 4] has a 1.6σ tension [5] with SM predictions. Furthermore, measurements in various di-muon invariant mass-squared (q^2) bins of $BR(B_s \rightarrow \phi \mu^+ \mu^-)$ are up to 4σ smaller than the SM predictions [6, 7]. Some angular distributions in $B \rightarrow K^* \mu^+ \mu^-$ decays have been measured by LHC experiments [8–13] to be several σ short of state-of-the-art SM predictions and the same can be said of $BR(B \rightarrow K^* \mu^+ \mu^-)$ [14]. We call the aforementioned tensions the neutral current $b \rightarrow s \mu^+ \mu^-$ anomalies. It is tempting to suppose that the tensions could be explained by unaccounted-for new physics. It has been shown in fits [15, 16] to measurements that the weak effective theory (WET) operators

$$\mathcal{L} = \dots + N \left(C_9^{(\mu)} (\bar{b} \gamma^\alpha P_L s) (\bar{\mu} \gamma_\alpha \mu) + C_{10}^{(\mu)} (\bar{b} \gamma^\alpha P_L s) (\bar{\mu} \gamma_\alpha \gamma_5 \mu) + H.c. \right) \quad (1.1)$$

parameterising the effects of new physics states significantly improve the situation. Such beyond-the-SM operators may be generated by integrating out putative heavy new physics states. Here, b is the bottom quark field, μ the muon field and s the strange quark field.

$N := 4G_F e^2 |V_{ts}| / (16\pi^2 \sqrt{2})$ is a normalising constant, where G_F is the Fermi decay constant, e the electromagnetic gauge coupling and V_{ij} the entries of the CKM matrix.

We use the `smelli2.3.2` [17] to predict the aforementioned $b \rightarrow s\mu^+\mu^-$ anomalies. `smelli2.3.2` puts them in the ‘quarks’ category of observable. For these, there is some debate about the most accurate predictions and the size of the associated theoretical uncertainties although many estimates (e.g. [18, 19]) predict that the size of the theoretical uncertainties alone cannot explain the $b \rightarrow s\mu^+\mu^-$ anomalies¹.

Contrary to the $b \rightarrow s\mu^+\mu^-$ anomalies, a 2022 LHCb reanalysis [23] holds that measurements of

$$R_A(q_{\min}^2, q_{\max}^2) := \frac{\int_{q_{\min}^2}^{q_{\max}^2} dq^2 BR(B \rightarrow A\mu^+\mu^-(q^2))}{\int_{q_{\min}^2}^{q_{\max}^2} dq^2 BR(B \rightarrow Ae^+e^-(q^2))}, \quad (1.2)$$

are broadly *compatible* with SM predictions for $A \in \{K, K^*\}$, within uncertainties². Such ratios are commonly called lepton flavour universality (LFU) variables. Since we entertain the possibility that the $b \rightarrow s\mu^+\mu^-$ anomalies may be pointing to some new physics state coupling to muons (and $\bar{b}s$ quarks) the reanalysis suggests that there should be also be a new physics contribution from

$$\mathcal{L} = \dots + N \left(C_9^{(e)} (\bar{b}\gamma^\alpha P_L s) (\bar{\mu}\gamma_\alpha \mu) + C_{10}^{(e)} (\bar{b}\gamma^\alpha P_L s) (\bar{\mu}\gamma_\alpha \gamma_5 \mu) + H.c. \right). \quad (1.3)$$

This possibility has already been partially addressed in Ref. [15], where constraints on the $C_9^{(e)} - C_9^{(\mu)}$ parameter plane from some different relevant flavour observables were presented, where all other new physics Wilson coefficients are null. It was demonstrated that there is parameter space where the constraints are compatible with each other at the 95% confidence level (CL). Some cases with other non-zero new physics Wilson operators were also analysed in Refs. [15, 16]). We note here that often, the natural language to describe the interactions of models is the SM effective field theory (SMEFT) [25], which involves complete representations of the unbroken SM gauge group (e.g. $SU(2)_L$ doublets), as opposed to weak effective theory, which is valid below the W boson mass.

In the following section, we shall perform our own fits including the new physics operators in (1.1) and (1.3). Then, in §3, we examine Z' models that are capable of predicting them, as well as other operators. Some of the other operators predict a change to predictions of di-lepton production cross-section measurements at experiments at the LEP-2 collider, which we recalculate in §4. Using these constraints, we examine the fits to our set of models in §5, quantifying the extent to which a coupling of the Z' to di-electron pairs is preferred. One particular model based on $U(1)_{3B_3-L_e-2L_\mu}$ is singled out as being close-to-optimal while

¹Some estimates in Ref. [20] fit an unidentified non-perturbative SM contribution that mimics a q^2 -dependent lepton-family universal C_9 in tandem with the new physics operators. Note also that the $b \rightarrow s\mu^+\mu^-$ anomalies persist when one uses ratios of observables including $\Delta M_{s,d}$, ϵ_K , $S_{\psi K_S}$ to cancel their dependence on CKM matrix elements [21, 22], although throughout the present paper, new physics contributions to CKM matrix elements are predicted to be negligible.

²There are some 1σ mild tensions, however, for $A = K_S^0$ and $A = K^{*\pm}$ [24].

having relatively low $U(1)$ charges for the fermionic fields. Parameter space constraints are included. We summarise and conclude in §6.

2 SMEFT operator fit

Introducing operators that couple di-electron and di-muon pairs with new physics appears to significantly improve fits to recent measurements. In Section 5 we investigate the best fit for Z' models described in Section 3, but to inform our choice of model we first understand the phenomenological effects of adding only four non-zero WCs: $C_9^{(e)}$, $C_9^{(\mu)}$, $C_{10}^{(e)}$ and $C_{10}^{(\mu)}$. We assume here that all other WCs are zero, and in this parameter space check how $b \rightarrow s\mu^+\mu^-$ measurements and LFU observables, especially the R_K and R_{K^*} ratios from the 2022 LHCb reanalysis [23], affect the statistical preference (or otherwise) for new physics that couples to di-electron pairs.

We place constraints and perform global fits in the parameter plane $C_9^{(e)} - C_9^{(\mu)}$ similar to Ref. [15]. Our evaluation focuses on four cases which encompass combinations of left-handed ($C_9^a = -C_{10}^a$ for $a \in \{e, \mu\}$) and vector-like ($C_{10}^a = 0$) couplings of new physics to di-muon pairs and/or di-electron pairs through appropriate selection of our chosen WCs. We shall take two-dimensional slices through the four-dimensional parameter space using combinations of these couplings.

The WCs introduced above belong to the weak effective theory, whereas `smelli2.3.2` requires inputs belonging to the Standard Model effective field theory (SMEFT). The SMEFT provides a framework for describing new physics contributions at energies much larger than the electroweak scale. We match between the weak effective Hamiltonian and the SMEFT operators as described in Ref. [20], and normalise by the constant N introduced in (1.1) to a new physics scale of 30 TeV. In our analysis of new physics that couples to di-muon pairs, the relevant SMEFT coefficients are denoted $C_{qe}^{(l)2322}$ and $C_{lq}^{(l)2223}$, which are input to `smelli2.3.2` in units of GeV^{-2} and are obtained from $C_9^{(\mu)}$ and $C_{10}^{(\mu)}$ by:

$$C_{qe}^{(l)2322} = 2N(C_9^{(\mu)} + C_{10}^{(\mu)}), \quad (2.1)$$

$$C_{lq}^{(l)2223} = 2N(C_9^{(\mu)} - C_{10}^{(\mu)}). \quad (2.2)$$

These are WCs multiplying the dimension-6 SMEFT operators in the Lagrangian density:

$$O_{qe}^{(l)2322} = (\bar{Q}_2\gamma_\alpha Q_3)(\bar{e}_2\gamma^\alpha e_2), \quad (2.3)$$

$$O_{lq}^{(l)2223} = (\bar{L}_2\gamma_\alpha L_2)(\bar{Q}_2\gamma^\alpha Q_3), \quad (2.4)$$

where L_i and Q_i are $SU(2)_L$ doublets and e_i singlets. We adapt Eqs. 2.1 - 2.4 to write the equivalent SMEFT coefficients and operators contributing to the transitions $b \rightarrow se^+e^-$, by replacing indices $2 \rightarrow 1$ on lepton doublets and singlets and $\mu \rightarrow e$ on weak effective theory coefficients on the right hand sides, in which case the left hand sides read $C_{qe}^{(l)2311}$, $C_{lq}^{(l)1123}$, $O_{qe}^{(l)2311}$ and $O_{lq}^{(l)1123}$, respectively.

We examine constraints from two main categories of observables contained in `smelli2.3.2`, labelled ‘quarks’ and ‘LFU’. The LFU category consists of 23 measurements from Belle, LHCb and BaBar which include constraints from the ratios R_K and R_{K^*} (which were updated by LHCb in 2022). We aim to understand to which extent this update favours adding new physics couplings to di-electron pairs. Therefore, we additionally examine these two LFU ratios separately from the total set of LFU contributions in our results. The ‘quarks’ category contains 224 other contributions from LHCb measurements of B meson decays and other similar measurements from ATLAS, CMS, Belle and BaBar.

The `smelli2.3.2` package requires several tools for performing a phenomenological analysis, including `flavio2.3.3` for computing flavour and other precision observables and accounting for their theory uncertainties, alongside `wilson2.3.2` for matching between the weak effective theory and the SMEFT and performing the renormalisation group running. The combination of these and other tools allows `smelli2.3.2` to produce a SMEFT likelihood function including a total of 247 observables to compare with predictions [26].

Our global fits aim to identify disparity between the combined measurements and predicted contributions from non-zero WCs by performing a χ^2 test (as described in Ref. [27]). Combined measurements include all available data from as many relevant sectors of experimental physics as possible, including B , Higgs and top physics, and LFU violating observables. The global SMEFT likelihood is necessary for taking into account the mixing between different sectors under renormalisation, as well as the complication that deviations in observables related to the B anomalies are possibly explained by models such as those adding a Z' that tend to predict additional effects in other observables. However, those observables with renormalisation group effects that are negligible in our parameter space are switched off in our global fits, as they contribute no difference to this analysis.

A similar fit to one of the four that we present in this section has also been performed (with a different set of b -observables and a different calculation of the SM prediction) in Ref. [15].

2.1 Fit results

In our first scenario, we set $C_{10}^{(e)} = C_{10}^{(\mu)} = 0$ and allow $C_9^{(e)}$ and $C_9^{(\mu)}$ to vary freely, corresponding to the case where new physics has vector-like couplings to both di-muon and di-electron pairs. The result is plotted in Fig. 1 (top-left). A significant region of overlap exists between the ‘LFU’ and ‘quarks’ constraints where $C_9^{(e)}$ takes values between around -1 and its SM value of 0. The most constraining observables from the collection of 23 that test lepton flavour universality appear to be ‘ R_K, R_{K^*} ’. This fit was performed by Ref. [15], and our fit shows broad agreement.

The second scenario we consider here requires $C_9^{(e)} = -C_{10}^{(e)}$ and $C_9^{(\mu)} = -C_{10}^{(\mu)}$ such that di-electron and di-muon pairs have only left-handed couplings with new physics, leaving a smaller range of best-fit values for $C_9^{(e)}$ as shown in Fig. 1 (top-right).

Another possibility we consider is that of vector-like couplings to di-electron pairs and left-handed couplings of new physics to di-muon pairs, presented in Fig. 1 (bottom-left). The

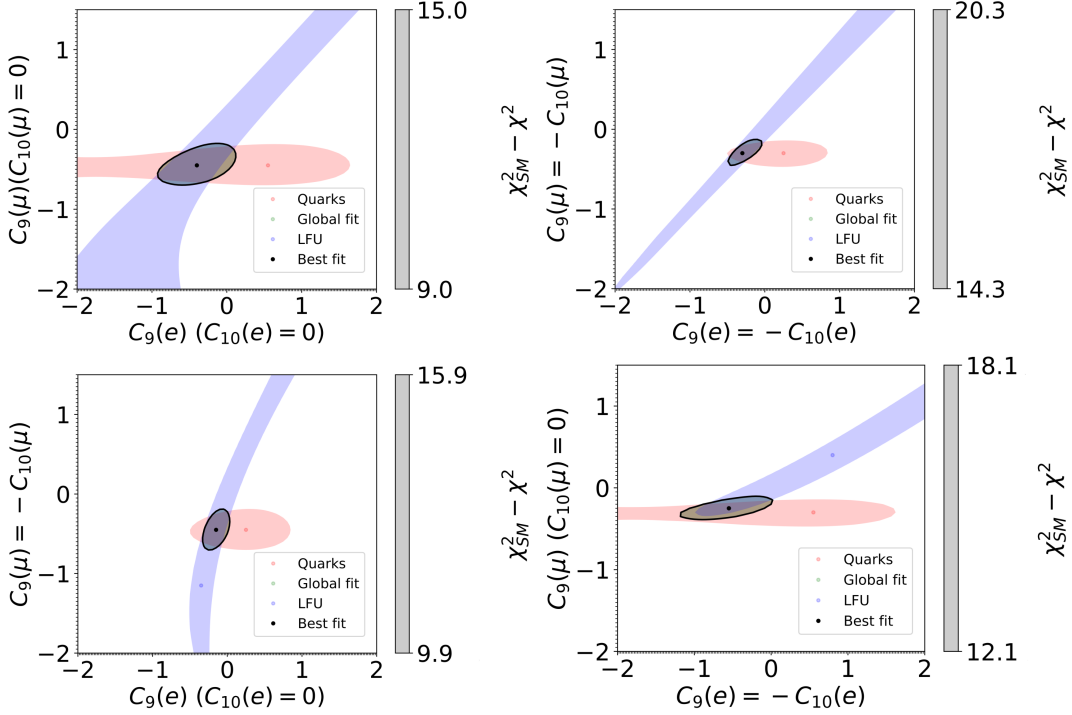


Figure 1. 95% confidence level (CL) fit regions in the parameter space where (top-left) $C_{10}^{(e)} = C_{10}^{(\mu)} = 0$, (top-right) $C_9^{(\mu)} = -C_{10}^{(\mu)}$ and $C_9^{(e)} = -C_{10}^{(e)}$, (bottom-left) $C_{10}^{(e)} = 0$ and $C_9^{(\mu)} = -C_{10}^{(\mu)}$, (bottom-right) $C_9^{(e)} = -C_{10}^{(e)}$ and $C_{10}^{(\mu)} = 0$. χ^2 improvement with respect to that of the SM as a function of electron charge divided by muon charge, X_e/X_μ . A positive value of $\chi^2_{SM} - \chi^2$ indicates an *improvement* of the fit with respect to the SM whereas a negative value indicates a worse fit than the SM. ‘LFU’ contains 23 measurements from Belle, LHCb and BaBar which test lepton flavour universality. ‘quarks’ contains the 224 other $b \rightarrow s\mu^+\mu^-$ measurements defined in flavio2.3.3. The grey colour bar on the right-hand side is labelled with the extremes of the $\chi^2_{SM} - \chi^2$ values within the 95% ‘global’ contour. The best fit is shown by the black point.

range of best-fit values for $C_9^{(e)}$ is similar here to that in the top-right panel, but this third scenario includes a wider range of best-fit values for $C_9^{(\mu)}$.

The fourth scenario we consider is Fig. 1 (bottom-right) where the couplings to new physics are swapped compared with the third scenario in the bottom-left panel such that di-electron pairs have left-handed couplings and di-muon pairs have vector-like couplings. A larger range of good-fit values for $C_9^{(e)}$ result for this scenario, and it is the only case with a fit that includes values extending below $C_9^{(e)} = -1$.

The main outcome of Ref. [15] is to evaluate global fits with and without new physics contributions to electron modes under a framework containing updates to both experimental measurements and theoretical calculations of form factors. Within this fully updated framework, their results identify that new physics introduced by $C_9^{(\mu)}$ is preferred over scenarios with $C_9^{(\mu)} = -C_{10}^{(\mu)}$, favouring vector or axial-vector operators. The fit also reveals that data

can be compatible with non-zero $C_{10}^{(\mu)}$, although support for these scenarios is not as strong. In particular, the analysis identifies that new physics scenarios with $C_9^{(\mu)} = -C_{10}^{(\mu)}$ may be indicated by charged current anomalies.

Other analyses support the introduction of non-zero new physics Wilson operators, though with different approaches. For example, a recent evaluation including possible new physics WCs [16] performed higher dimensional global fits for a several more non-zero WCs instead of focusing on the four that we examine here. There is therefore no overlap between our results and those of Ref. [16].

Both Refs. [15] and [16] provide insight into the a renewed focus on LFU new physics by examining the differences between global fits before and after the release of the 2022 LHCb update of R_K and R_{K^*} . The large impact of these two observables on constraining the parameter plane $C_9^{(e)} - C_9^{(\mu)}$ is clear from Fig. 1.

Fig. 1 indicates that $C_9^{(e)} = C_9^{(\mu)} \neq 0$ is close to the most-favoured point in two-dimensional slices of parameter space, but that $C_9^{(e)} = 0$ can also fit the data, as shown in the top-left hand panel. Motivated by this top-left hand panel, we shall now turn to a set of models which interpolates between $C_9^{(e)} = C_9^{(\mu)} \neq 0$ and $C_9^{(e)} = 0$ (and which extrapolates outside of these conditions).

3 Models

Our $U(1)_X$ gauge symmetry is expected to be spontaneously broken by a complex scalar ‘flavon’ field θ , whose $U(1)_X$ charge Q is non-zero. Of the models we shall propose, aspects such as these are very similar to the $U(1)_{B_3-L_2}$ model [28], Third Family Hypercharge models [29, 30] or mixtures between the two [31]. The massive electrically neutral gauge boson resulting from Higgsed $U(1)_X$ breaking is dubbed a Z' boson which has a mass

$$M_{Z'} = Qg_{Z'}\langle\theta\rangle, \quad (3.1)$$

where $\langle\theta\rangle$ is the vacuum expectation value of the flavon field. Whichever fields possess non-zero $U(1)_X$ charges will generically have couplings to the Z' boson. Thus we wish second-family leptons to have a non-zero charge, and (following the arguments in §1), possibly first-family leptons as well. We also wish the third family of quarks to have a charge in order to establish a Z' coupling to $s\bar{b} + H.c.$, starting from a coupling to $b\bar{b}$ in the weak eigenbasis, as also explained in §1. Then, we may explain the $b \rightarrow s\ell^+\ell^-$ anomalies by new physics contributions to the amplitude like the one depicted in Fig. 2. It should be evident from the above discussion that the charges of the various fields in the model affect the phenomenology of it, since they determine what the Z' couples to (and with which relative strength). Therefore, we now discuss the fermionic charge assignment of the model.

3.1 Fermionic charge assignment

We begin by extending the SM by three right-handed neutrino fields ν_i . These ν_i fields will be used both for anomaly cancellation and, ultimately, with an eye to providing an ultra-

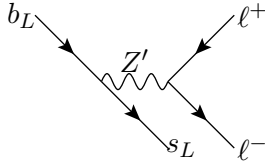


Figure 2. Feynman diagram of the leading new physics contribution to $b \rightarrow s\ell^+\ell^-$ observables from a suitable Z' model.

Field	$(SU(3), SU(2), U(1)_Y, U(1)_X)$
Q_i	$(3, 2, 1, Q_i)$
L_i	$(1, 2, 3, L_i)$
u_i	$(3, 1, 4, u_i)$
d_i	$(3, 1, -2, d_i)$
e_i	$(1, 1, -6, e_i)$
ν_i	$(1, 1, 0, \nu_i)$

Table 1. Representations of fermionic chiral fields under the $SM \times U(1)_X$ gauge group. $i \in \{1, 2, 3\}$ is a family index and gauge indices have been suppressed. Q_i and L_i are left-handed Weyl fermions, whereas the other fields listed are all right-handed Weyl fermions. We have chosen here to normalise the hypercharge gauge coupling so that the hypercharges of all fermionic fields are integers.

violet model of neutrino masses (this we shall not specify in any detail, however). The chiral fermionic field content of the model and its representations under the $SM \times U(1)_X$ gauge group is specified in Table 1. We note here that for brevity we shall denote both the field and its $U(1)_X$ charge by the same label; context should make the meaning of the symbol clear.

As explained above, we want to find a set of models that can potentially address the $b \rightarrow s\mu^+\mu^-$ anomalies, but which interpolate between models where the Z' does *not* couple to electrons and those where it couples with an equal strength to di-electron pairs and di-muon pairs. However, the $U(1)_X$ charge assignments have constraints upon them given by the requirement of not generating quantum field theoretic anomalies, which would spoil the gauge symmetry. We shall now go through the arguments that lead us to the charge assignments, since they shall make clear to which extent the assignments are constrained by anomaly cancellation, to which extent they are a choice dictated by desired phenomenology and to which extent they are just a choice to be concrete.

We first list the anomaly cancellation conditions which a gauged $U(1)_X$ chiral-fermion

charge assignment should respect [32]:

$$\sum_i (2Q_i - u_i - d_i) = 0, \quad (3.2)$$

$$\sum_i (L_i + 3Q_i) = 0, \quad (3.3)$$

$$\sum_i (Q_i + 3L_i - 8u_i - 2d_i - 6e_i) = 0, \quad (3.4)$$

$$\sum_i (6Q_i + 2L_i - 3u_i - 3d_i - e_i - \nu_i) = 0, \quad (3.5)$$

$$\sum_i (Q_i^2 - L_i^2 - 2u_i^2 + d_i^2 + e_i^2) = 0 \quad (3.6)$$

$$\sum_i (6Q_i^3 + 2L_i^3 - 3u_i^3 - 3d_i^3 - e_i^3 - \nu_i^3) = 0. \quad (3.7)$$

These equations have been simultaneously solved over the integers both numerically with $U(1)_X$ charges between 10 and -10 [32] and, more generally, analytically [33]. Rather than begin with these solutions and then restrict them, we instead find it instructive to make some choices based partly on expected phenomenological consequences of some charge assignments whilst simultaneously applying (3.2)-(3.7).

We require a coupling of the Z' to left-handed $b\bar{s}$ quark pairs in order to explain an apparent new physics effect in $b \rightarrow s\mu^+\mu^-$ transitions. We therefore pick $Q_3 \neq 0$, providing a Z' coupling to left-handed $b\bar{b}$ pairs and assume that its coupling to (left-handed) $barbs + H.c.$ will be provided by some small amount of $b - s$ mixing. The mixing is banned by $U(1)_X$ but since this is spontaneously broken, we anticipate small $U(1)_X$ breaking effects, such as small quark mixing. We may fix $Q_3 = 1$ by rescaling the $U(1)_X$ gauge coupling. If we couple the Z' dominantly to the *third* family quarks only, direct Z' search bounds from the LHC will be weaker, since LHC Z' production dominantly occurs via the $b\bar{b} \rightarrow Z'$ process, which is doubly suppressed by both the b and \bar{b} parton distribution functions. Motivated by this, we fix the $U(1)_X$ charges of the first two generations of quark fields to zero, i.e. $u_1 = u_2 = d_1 = d_2 = Q_1 = Q_2 = 0$. Substituting these assignments into (3.2), we obtain that $u_3 + d_3 = 2$. We shall here pick $u_3 = d_3 = 1$, meaning that we can characterise the quark charges in terms of third-family baryon number. (3.3) then gives that

$$\sum_i L_i = -3. \quad (3.8)$$

We shall pick $L_2 \neq 0$ in order to couple the Z' to left-handed muon pairs, since we know from fits to $b \rightarrow s\mu^+\mu^-$ anomalies [15, 16] that this coupling is necessary to describe them well. We shall vary L_1 in order to vary the Z' coupling to left-handed electron pairs: (3.8) then can be rearranged to yield L_3 . Substituting (3.8) and the other assigned charges into (3.4), we obtain

$$\sum_i e_i = -3, \quad (3.9)$$

which allows us to obtain, using (3.5),

$$\sum_i \nu_i = -3. \quad (3.10)$$

(3.6) and (3.7) then become

$$\sum_i (L_i^2 - e_i^2) = 0, \quad (3.11)$$

$$\sum_i (2L_i^3 - e_i^3 - \nu_i^3) = 0. \quad (3.12)$$

(3.8)-(3.12) are solved by

$$L_i = e_i = \nu_i \text{ for each } i; \quad (3.13)$$

which is not a general solution of the equations, but which is sufficient for our purposes here. After the stipulation in (3.13), there remains only one independent constraint, which we can take to be (3.8). (3.13) allows us to summarise the $U(1)_X$ charges in terms of electron number L_e , muon number L_μ and tau number L_τ . We shall fix the X charge of $L_2 = e_2 = \nu_2$ to a relatively large integer to allow more resolution in the other charges (here, we pick it to be 10). We then allow the $U(1)_X$ electron charge $-X_e$ to vary. The $U(1)_X$ charges of the fermions as a whole can be characterised by

$$3B_3 - (X_e L_e + X_\mu L_\mu + [3 - X_e - X_\mu] L_\tau). \quad (3.14)$$

$X_e/X_\mu = 1$ corresponds to the case where the coupling of the Z' to di-electron pairs is equal to that of di-muon pairs, whereas $X_e = 0$ is the case where the electron does not directly couple to the Z' at tree-level.

We fix the $U(1)_X$ charge of the SM Higgs doublet H so that the top Yukawa coupling Lagrangian density term, $\lambda_t \overline{Q}_3 H u_3 + H.c.$, is allowed by the gauge symmetry³. This constraint requires that H then has $U(1)_X$ charge equal to zero, simplifying our analysis because there is no predicted $Z - Z'$ mixing at tree-level. Such a mixing would change the predictions of electroweak precision observables; with zero mixing, as predicted here, we effectively decouple the electroweak precision observables from our discussion. It behoves us to specify the other pertinent TeV-scale properties of our model, which we shall do in the subsequent subsection.

3.2 More model details

Here, we deal with the Z' -specific parts of the model, which encapsulates the phenomenology that we are interested in predicting. We shall not find it necessary to specify all details of the model (the flavon potential or flavon/Higgs mixing – for that, see Ref. [35] – or the origin of *non-zero* small Yukawa couplings, for example). The model set-up in the present subsection

³Some of the other Yukawa couplings may be disallowed by $U(1)_X$, but may receive small contributions from non-renormalisable operators (for example as in the Froggatt-Nielsen mechanism [34]) once $U(1)_X$ is spontaneously broken.

closely follows that of Refs. [28–31], which are discriminated from the present model by the fermionic $U(1)_X$ charge assignments. The model is supposed to be at the level of a TeV-scale effective field theory that includes the quantum fields of the SM, three right-handed neutrino fields and the Z' . We write the fermionic fields in the gauge eigenbasis with a primed notation

$$\begin{aligned} \mathbf{u}'_{\mathbf{L}} &= \begin{pmatrix} u'_L \\ c'_L \\ t'_L \end{pmatrix}, & \mathbf{d}'_{\mathbf{L}} &= \begin{pmatrix} d'_L \\ s'_L \\ b'_L \end{pmatrix}, & \mathbf{e}'_{\mathbf{L}} &= \begin{pmatrix} e'_L \\ \mu'_L \\ \tau'_L \end{pmatrix}, & \boldsymbol{\nu}'_L &= \begin{pmatrix} \nu'_{eL} \\ \nu'_{\mu L} \\ \nu'_{\tau L} \end{pmatrix}, \\ \mathbf{u}'_{\mathbf{R}} &= \begin{pmatrix} u'_R \\ c'_R \\ t'_R \end{pmatrix}, & \mathbf{d}'_{\mathbf{R}} &= \begin{pmatrix} d'_R \\ s'_R \\ b'_R \end{pmatrix}, & \mathbf{e}'_{\mathbf{R}} &= \begin{pmatrix} e'_R \\ \mu'_R \\ \tau'_R \end{pmatrix}, & \boldsymbol{\nu}'_R &= \begin{pmatrix} \nu'_{eR} \\ \nu'_{\mu R} \\ \nu'_{\tau R} \end{pmatrix}, \end{aligned} \quad (3.15)$$

along with the SM fermionic electroweak doublets

$$\mathbf{Q}'_i = \begin{pmatrix} \mathbf{u}'_{\mathbf{L}i} \\ \mathbf{d}'_{\mathbf{L}i} \end{pmatrix}, \quad \mathbf{L}'_i = \begin{pmatrix} \boldsymbol{\nu}'_{\mathbf{L}i} \\ \mathbf{e}'_{\mathbf{L}i} \end{pmatrix}. \quad (3.16)$$

The neutrinos and SM fermions acquire masses after the SM Brout-Englert-Higgs mechanism through

$$-\mathcal{L}_Y = \overline{\mathbf{Q}'} Y_u \tilde{H} \mathbf{u}'_{\mathbf{R}} + \overline{\mathbf{Q}'} Y_d H \mathbf{d}'_{\mathbf{R}} + \overline{\mathbf{L}'} Y_e H \mathbf{e}'_{\mathbf{R}} + \overline{\mathbf{L}'} Y_\nu \tilde{H} \boldsymbol{\nu}'_R + \frac{1}{2} \overline{\boldsymbol{\nu}'_R{}^c} M \boldsymbol{\nu}'_R + H.c., \quad (3.17)$$

where Y_u , Y_d and Y_e are dimensionless complex coupling constants, each written as a 3 by 3 matrix in family space; the matrix M is a 3 by 3 complex symmetric matrix of mass dimension 1, Φ^c denotes the charge conjugate of field Φ and $\tilde{H} := (H^{0*}, -H^-)^T$. Gauge indices have been omitted in (3.17).

For $X_e \neq X_\mu \neq X_\tau$, the Yukawa couplings have the following textures at the renormalisable tree level in the unbroken $U(1)_X$ limit:

$$Y_u \sim \begin{pmatrix} \times & \times & 0 \\ \times & \times & 0 \\ 0 & 0 & \times \end{pmatrix}, \quad Y_d \sim \begin{pmatrix} \times & \times & 0 \\ \times & \times & 0 \\ 0 & 0 & \times \end{pmatrix}, \quad Y_e \sim \begin{pmatrix} \times & 0 & 0 \\ 0 & \times & 0 \\ 0 & 0 & \times \end{pmatrix}. \quad (3.18)$$

The structure of Y_e predicts that charged-lepton violating couplings of the Z' are zero.

We may write $H = (0, (v+h)/\sqrt{2})^T$ after electroweak symmetry breaking, where h is the physical Higgs boson field and (3.17) includes the fermion mass terms

$$\begin{aligned} -\mathcal{L}_Y &= \overline{\mathbf{u}'_{\mathbf{L}}} V_{uL} V_{uL}^\dagger m_u V_{uR} V_{uR}^\dagger \mathbf{u}'_{\mathbf{R}} + \overline{\mathbf{d}'_{\mathbf{L}}} V_{dL} V_{dL}^\dagger m_d V_{dR} V_{dR}^\dagger \mathbf{d}'_{\mathbf{R}} + \overline{\mathbf{e}'_{\mathbf{L}}} V_{eL} V_{eL}^\dagger m_e V_{eR} V_{eR}^\dagger \mathbf{e}'_{\mathbf{R}} + \\ &\frac{1}{2} (\overline{\boldsymbol{\nu}'_L} \boldsymbol{\nu}'_R{}^c) M_\nu \begin{pmatrix} \boldsymbol{\nu}'_L{}^c \\ \boldsymbol{\nu}'_R \end{pmatrix} + H.c. + \dots, \end{aligned} \quad (3.19)$$

where

$$M_\nu = \begin{pmatrix} 0 & m_{\nu D} \\ m_{\nu D}^T & M \end{pmatrix}, \quad (3.20)$$

V_{I_L} and V_{I_R} are 3 by 3 unitary mixing matrices for each field species I , $m_u := vY_u/\sqrt{2}$, $m_d := vY_d/\sqrt{2}$, $m_e := vY_e/\sqrt{2}$ and $m_{\nu_D} := vY_\nu/\sqrt{2}$, where v is the SM Higgs expectation value, measured to be 246.22 GeV [36]. The final explicit term in (3.19) incorporates the see-saw mechanism via a 6 by 6 complex symmetric mass matrix. Since the elements in m_{ν_D} are much smaller than those in M , we perform a rotation to obtain a 3 by 3 complex symmetric mass matrix for the three light neutrinos. These approximately coincide with the left-handed weak eigenstates ν'_L , whereas three heavy neutrinos approximately correspond to the right-handed weak eigenstates ν'_R . The neutrino mass term of (3.19) becomes, to a good approximation,

$$-\mathcal{L}_\nu = \frac{1}{2}\overline{\nu'_L}{}^c m_\nu \nu'_L + \frac{1}{2}\overline{\nu'_R}{}^c M \nu'_R + H.c., \quad (3.21)$$

where $m_\nu := m_{\nu_D}^T M^{-1} m_{\nu_D}$ is a complex symmetric 3 by 3 matrix.

Choosing $V_{I_L}^\dagger m_I V_{I_R}$ to be diagonal, real and positive for $I \in \{u, d, e\}$, and $V_{\nu_L}^T m_\nu V_{\nu_L}$ to be diagonal, real and positive (all in ascending order of mass from the top left toward the bottom right of the matrix), we can identify the *non-primed mass eigenstates*⁴

$$\mathbf{P} = V_P^\dagger \mathbf{P}' \text{ where } P \in \{u_R, d_L, u_L, e_R, u_R, d_R, \nu_L, e_L\}. \quad (3.22)$$

We may then find the CKM matrix V and the Pontecorvo-Maki-Nakagawa-Sakata (PMNS) matrix U in terms of the fermionic mixing matrices:

$$V = V_{u_L}^\dagger V_{d_L}, \quad U = V_{\nu_L}^\dagger V_{e_L}. \quad (3.23)$$

The zeroes in Y_u and Y_d in (3.18) predict that the magnitudes of the elements $V_{23}, V_{13}, V_{32}, V_{31}$ are much smaller than 1, agreeing with measurements [36]. Clearly, more model building into the ultra-violet would be required to understand the details of neutrino masses and mixings and how exactly the zeroes in (3.18) are filled in with small entries. We leave such model considerations aside, instead pointing to §2.5 of Ref. [5] for some possibilities.

The kinetic terms of the $U(1)_X$ boson lead to the following Z' interactions

$$\mathcal{L} = -g_{Z'} \left(\overline{\mathbf{Q}}' Z' \xi \mathbf{Q}' + \overline{\mathbf{u}}'_R Z' \xi \mathbf{u}'_R + \overline{\mathbf{d}}'_R Z' \xi \mathbf{d}'_R + \overline{\mathbf{L}}' Z' \Xi \mathbf{L}' + \overline{\mathbf{e}}'_R Z' \Xi \mathbf{e}'_R + \overline{\nu}'_R Z' \Xi \nu'_R \right), \quad (3.24)$$

where

$$\xi := \begin{pmatrix} 0 & 0 & 0 \\ 0 & 0 & 0 \\ 0 & 0 & 1 \end{pmatrix}, \quad \Xi := \begin{pmatrix} -X_e & 0 & 0 \\ 0 & -X_\mu & 0 \\ 0 & 0 & -X_\tau \end{pmatrix} \quad (3.25)$$

are fixed by the fermionic fields' $U(1)_X$ charges. The right-handed neutrinos ν'_R are assumed to be heavy compared to the TeV scale and play no further role in the phenomenology of $b \rightarrow s\mu^+\mu^-$ anomalies; we shall therefore neglect them in the discussion that follows. In the unprimed mass eigenbasis, (3.24) becomes

$$\mathcal{L} = -g_{Z'} \left(\overline{\mathbf{u}}_L Z' \lambda_\xi^{uL} \mathbf{u}_L + \overline{\mathbf{d}}_L Z' \Lambda_\xi^{dL} \mathbf{d}_L + \overline{\mathbf{u}}_R Z' \Lambda_\xi^{uR} \mathbf{u}_R + \overline{\mathbf{d}}_R Z' \Lambda_\xi^{dR} \mathbf{d}_R + \overline{\mathbf{e}}_L Z' \Lambda_\Xi^{eL} \mathbf{e}_L + \overline{\mathbf{e}}_R Z' \Lambda_\Xi^{eR} \mathbf{e}_R + \overline{\nu}_L Z' \Lambda_\Xi^{\nu L} \nu_L \right), \quad (3.26)$$

⁴ \mathbf{P} and \mathbf{P}' are column 3-vectors.

WC	value	WC	value
C_{ll}^{iiii}	$-\frac{1}{2}L_i^2$	$C_{ll}^{ijjj} (i \neq j)$	$-L_i L_j$
$(C_{lq}^{(1)})^{ijk}$	$L_i(\Lambda_{\Xi}^{(d_L)})_{jk}$	C_{ee}^{iiii}	$-\frac{1}{2}L_i^2$
$C_{ee}^{ijjj} (i \neq j)$	$-L_i L_j$	C_{uu}^{3333}	$-\frac{1}{2}$
C_{eu}^{ii33}	L_i	C_{ed}^{ii33}	L_i
$C_{ud}^{(1)3333}$	1	C_{le}^{ijjj}	$L_i L_j$
C_{qe}^{ijkk}	$L_k(\Lambda_{\Xi})_{ij}$	$C_{qu}^{(1)ij33}$	$-(\Lambda_{\Xi})_{ij}$

Table 2. Non-zero $M_{Z'}$ -scale SMEFT operators in units of $g_{Z'}/M_{Z'}$, in terms of the left-handed lepton doublet $U(1)_X$ charges L_i . The notation is in the down-aligned Warsaw basis [25]. There is no sum implied upon repeated family indices $i, j, k \in \{1, 2, 3\}$.

where $\Lambda_{\alpha}^P := V_P \alpha V_P^{\dagger}$ for $P \neq \nu_L$ and $\alpha \in \{\xi, \Xi\}$. $\Lambda_{\alpha}^{\nu} := V_P \alpha V_P^T$

To make phenomenological progress with our models, we shall need to specify V_P . We simply assume that the ultra-violet model details are such that the zeroes in (3.18) are filled in (or not) at the correct level for experiment. The V_P are 3 by 3 unitary matrices, and we pick a simple ansatz which is not immediately obviously ruled out by strong flavour changing neutral current constraints on charged lepton flavour violation or neutral current flavour violation in the first two families of quark. Firstly, we set $V_{e_R} = V_{d_R} = V_{u_R} = V_{e_L} = I$, the 3 by 3 identity matrix. A non-zero $(V_{d_L})_{23}$ matrix element is required for the Z' to mediate new physics contributions to $b \rightarrow s \ell^+ \ell^-$ transitions. We capture the important quark mixing (i.e. between s_L and b_L) in V_{d_L} as

$$V_{d_L} = \begin{pmatrix} 1 & 0 & 0 \\ 0 & \cos \theta_{sb} & \sin \theta_{sb} \\ 0 & -\sin \theta_{sb} & \cos \theta_{sb} \end{pmatrix}. \quad (3.27)$$

V_{ν_L} and V_{u_L} are fixed by (3.23), where we use the experimentally determined values for the entries of V and U via the central values in the standard parameterisation from Ref. [36]. Having fixed all of the fermionic mixing matrices, we have provided an ansatz that could be perturbed around for a more complete characterisation. We leave such perturbations aside in the present paper.

Here, we summarise the SMEFT operators that result from integrating out the Z' ; they are given in Table 2, ready for input into `flavio2.3.3` [37]. We note that, to specify the model and its Z' phenomenology, once we have picked a value for X_e , there are three important model parameters that affect the pertinent phenomenology: $g_{Z'}$, $M_{Z'}$ and θ_{sb} , but at tree-level, as Table 2 shows, the flavour data only depend upon two effective parameters: the combination $g_{Z'}/M_{Z'}$ and θ_{sb} .

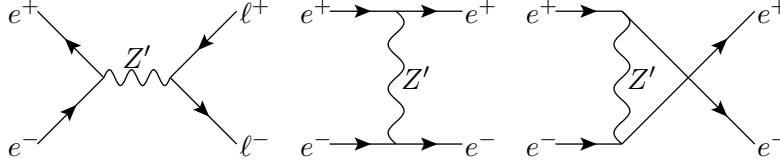


Figure 3. Feynman diagram of the leading Z' contribution to LEP-2 di-lepton production from a suitable model. Here, $\ell \in \{e, \mu, \tau\}$.

4 LEP constraints

Since some of the models we consider are couple the Z' to di-electron pairs, LEP-2 di-lepton production cross-section measurements, which are broadly in agreement with SM predictions, provide constraints. This is because a contribution from the Z' becomes non-zero: some leading Feynman diagrams for its contribution to the amplitude are shown in Fig. 3. In this section, we shall re-examine the constraints on four-lepton dimension-6 SMEFT WCs coming from LEP-2. Analytic expressions for the expected dominant contributions from these (in the interference terms) have been already calculated in Ref. [38]. Here, we re-calculate the full dependence of the tree-level predictions upon the WCs ready for inclusion into `flavio2.3.3`. By extracting the interference terms, we shall provide an independent check upon the analytic results presented in Ref. [38]. By calculating the *full* tree-level dependence upon the WCs (i.e. not only including the interference terms) and putting them into `flavio2.3.3`, we evade possible computational problems with predicted negative cross-sections when performing parameter scans. Ref. [38] provided numerical results of a fit to electroweak measurements of the epoch and other LEP measurements, where some of the WCs are constrained at the $\mathcal{O}(10^{-2})/v^2$ level, where $v = 246.22$ GeV is the SM Higgs vacuum expectation value. Although LEP experimental measurements have not changed since Ref. [38], some electroweak data have. Providing the LEP constraints as part of the `flavio2.3.3` package should then facilitate SMEFT fits in general as well as fits to our Z' models, once we have matched the model to SMEFT.

Some of the SMEFT WCs alter differential scattering cross-section predictions of $e^+e^- \rightarrow \mu^+\mu^-$, $e^+e^- \rightarrow \tau^+\tau^-$ and $e^+e^- \rightarrow e^+e^-$ (Bhabha scattering). In the Warsaw convention [25], the relevant WCs which can alter the predictions for these processes are C_{le}^{1jj1} , C_{ll}^{11jj} , C_{ee}^{11jj} , C_{le}^{11jj} and C_{le}^{11jj} , where $j \in \{1, 2, 3\}$. The predictions for $e^+e^- \rightarrow \mu^+\mu^-$ and $e^+e^- \rightarrow \tau^+\tau^-$ are simple and almost identical to each other and so we consider them first, before going on to consider Bhabha scattering.

4.1 LEP: di-muon and di-tau final states

Building notation similar to that in Ref. [39], we consider the tree-level polarised scattering amplitudes of massless di-electron pairs into either massless di-muon pairs ($j = 2$) or massless

di-tau pairs ($j = 3$) including 4-lepton dimension-6 SMEFT operators

$$\mathcal{M}\left(e^+e^- \rightarrow e_j^+e_j^-\right) = -i(\bar{e}\gamma^\alpha P_L e_j)(\bar{e}_j\gamma_\alpha P_R e)C_{le}^{1jj1} + i\sum_{X,Y}(\bar{e}\gamma^\alpha P_X e)(\bar{e}_j\gamma_\alpha P_Y e_j)N_{1jj1}^{XY}(s), \quad (4.1)$$

where the sum is over $\{X, Y\} \in \{L, R\}$,

$$N_{1jj1}^{XY}(s) := \frac{e^2}{s} + \frac{g_Z^{eX}g_Z^{eY}}{s - M_Z^2 + i\Gamma_Z M_Z} + \left(C_{ll}^{11jj} + C_{ll}^{1jj1}\right)\delta_{XL}\delta_{YL} + C_{ee}^{11jj}\delta_{XR}\delta_{YR} + C_{le}^{11jj}\delta_{XL}\delta_{YR} + C_{le}^{jj11}\delta_{XR}\delta_{YL}, \quad (4.2)$$

$\delta_{LL} = \delta_{RR} = 1$, $\delta_{LR} = \delta_{RL} = 0$, s, t and u are the usual Mandelstam kinematic variables, M_Z is the Z^0 boson pole mass and the SMEFT Wilson coefficients C_{ee}^{ijkm} , C_{le}^{ijkm} and C_{ll}^{ijkm} (where $i, j, k, m \in \{1, 2, 3\}$ are family indices) are written in the Warsaw convention [25]. g_Z^{eX} is the di- X -handed electron coupling to the Z^0 boson including tree-level corrections from SMEFT and g_Z^{eY} is the di- Y -handed j^{th} -family coupling to the Z^0 boson [40]. Γ_Z is the Z^0 boson's total width. Summing over the final spins and averaging over initial spins, we obtain a differential cross-section

$$\frac{d\sigma}{dt} = \frac{1}{16\pi} \left\{ |C_{le}^{1jj1}|^2 + \sum_{X,Y} |N_{1jj1}^{XY}(s)|^2 \left[\delta_{XY} \left(1 + \frac{t}{s}\right)^2 + (1 - \delta_{XY}) \frac{t^2}{s^2} \right] \right\}. \quad (4.3)$$

Integrating, we obtain the total cross-section

$$\sigma(e^+e^- \rightarrow e_j^+e_j^-) = \frac{s}{48\pi} \left\{ 3|C_{le}^{1jj1}|^2 + \sum_{X,Y} |N_{1jj1}^{XY}(s)|^2 \right\} \quad (4.4)$$

and a forward cross-section minus backward cross-section

$$\sigma(e^+e^- \rightarrow e_j^+e_j^-)_F - \sigma(e^+e^- \rightarrow e_j^+e_j^-)_B = \frac{s}{64\pi} \sum_{X,Y} |N_{1jj1}^{XY}(s)|^2 (2\delta_{XY} - 1). \quad (4.5)$$

The dimension-6 WC-SM interference terms in (4.4) and (4.5) agree with the interference terms derived in Ref. [38] (in the parameter space considered in Ref. [38], such interference terms encapsulate the dominant effects of the SMEFT operators and were the only ones presented explicitly there). (4.3) shows that the part proportional to $|C_{le}^{1jj1}|^2$ does not interfere with the rest of the matrix element due to its different helicity-flavour structure (as already noted in Ref. [38]).

In Ref. [41], the SM prediction for the cross-section is given including some higher-order one-loop contributions. By using the *ratio* of the predicted cross-section to the SM prediction in the constraints, we can effectively include the dominant effects of these higher order contributions. Our implementation in `flavio2.3.3` therefore uses such a ratio. Both

the ratios of the total cross-section and the forward cross-section minus the backward cross-section are used for the following LEP 2 centre-of-mass energies:

$$E/\text{GeV} \in \{130.3, 136.3, 161.3, 172.1, 182.7, 188.6, 191.6, 195.5, 199.5, 201.8, 204.8, 206.5\}. \quad (4.6)$$

Correlations between the various measurements are neglected for $e^+e^- \rightarrow \ell^+\ell^-$, where $\ell \in \{\mu, \tau\}$.

4.2 LEP: Bhabha scattering

We calculate the tree-level polarised amplitude \mathcal{M} for $e^+(p_2)e^-(p_1) \rightarrow e^+(q_2)e^-(q_1)$ in the massless electron approximation.

$$-i\mathcal{M} = -I_t \frac{e^2}{t} + I_s \frac{e^2}{s} + \sum_{X,Y} \left\{ -(\bar{u}\gamma^\mu P_X u)(\bar{v}\gamma_\mu P_Y v) t_{XY} + (\bar{u}\gamma^\mu P_X v)(\bar{v}\gamma_\mu P_Y u) s_{XY} \right\} \quad (4.7)$$

where $u := u(p_1)$, $v := v(q_2)$, $\bar{u} := \bar{u}(q_1)$ and $\bar{v} := \bar{v}(p_2)$ are the usual positive and negative energy 4-component Dirac spinors of the electron field and

$$\begin{aligned} I_t &:= (\bar{u}\gamma^\mu u)(\bar{v}\gamma_\mu v), \\ I_s &:= (\bar{u}\gamma^\mu v)(\bar{v}\gamma_\mu u), \\ t_{XY} &:= \frac{g_{e_X} g_{e_Y}}{t - M_Z^2 + i\Gamma_Z M_Z} + \frac{C_{XY} + C_{YX}}{2}, \\ s_{XY} &:= \frac{g_{e_X} g_{e_Y}}{s - M_Z^2 + i\Gamma_Z M_Z} + \frac{C_{XY} + C_{YX}}{2} \end{aligned} \quad (4.8)$$

and $C_{LL} := C_{ll}^{(1)1111}$, $C_{RR} := C_{ee}^{1111}$, $C_{LR} := C_{le}^{1111}$ and $C_{RL} := C_{le}^{1111}$. The spin summed/averaged differential cross-section in the centre-of-mass frame is then

$$\begin{aligned} \frac{d\sigma}{d\cos\theta} &= \frac{1}{32\pi s} \left(2e^4 \left[\frac{u^2 + t^2}{t^2} + \frac{u^2 + t^2}{s^2} + \frac{2u^2}{st} \right] + \right. \\ &\quad \sum_{X,Y} \left\{ \frac{2e^2}{t} (\text{Re}(t_{XY}) [u^2\delta_{XY} + s^2(1 - \delta_{XY})] + \text{Re}(s_{XY})u^2\delta_{XY}) + \right. \\ &\quad \frac{2e^2}{s} (\text{Re}(s_{XY}) [u^2\delta_{XY} + t^2(1 - \delta_{XY})] + \text{Re}(t_{XY})u^2\delta_{XY}) + \\ &\quad |t_{XY}|^2 [u^2\delta_{XY} + s^2(1 - \delta_{XY})] + |s_{XY}|^2 [u^2\delta_{XY} + t^2(1 - \delta_{XY})] + \\ &\quad \left. \left. 2\text{Re}(t_{XY}^\dagger s_{XY})u^2\delta_{XY} \right\} \right), \end{aligned} \quad (4.9)$$

where θ is the scattering angle. Extracting the dimension-6 SMEFT WC-SM interference terms from (4.9), we observe agreement with Ref. [38], providing an independent check on both calculations. In order to implement the Bhabha scattering constraints into `flavio2.3.3` we have integrated (4.9) with respect to $\cos\theta$ (utilising $t = -s(1 - \cos\theta)/2$ and $u = -s(1 + \cos\theta)/2$), since the combined LEP2 data in Ref. [41] are given in bins of $\cos\theta$. The resulting

expression is rather large, so we do not list it here, although we note that it can be found in the ancillary information stored with the `arXiv` version of this paper.

Ref. [41] combined LEP-experiment cross-sections for $e^+e^- \rightarrow e^+e^-$ for centre-of-mass energies between 189 GeV and 207 GeV and in bins of $\cos\theta$ in the interval $[-0.9, 0.9]$ were presented. The SM prediction of the binned cross-sections were also given and we again shall constrain the ratio of the measured cross-section to the SM prediction to constrain SMEFT operators. Here, correlations between measurements were given in Ref. [41] and are taken into account. We again take ratios of each measurement with the SM prediction in order to effectively utilise some higher order corrections that were included in the SM prediction; calculating their correlation coefficients, we see that these ratios have identical correlations to those between the original measurements, since the normalising factor cancels between the numerator and the denominator.

5 Fits

For each of the models in the set identified in §3, we perform a fit of θ_{sb} and $g_{Z'}/M_{Z'}$ to various data by using `smelli2.3.2` [17], `flavio2.3.3` [37] and `wilson2.3.2` [42] (to a good approximation broken only by small loop corrections, the WCs – and thus the predictions of observables which are affected by them – only depend upon the ratio $g_{Z'}/M_{Z'}$ rather than on $g_{Z'}$ and $M_{Z'}$ separately. Practically, in the numerics, we set $M_{Z'} = 3$ TeV throughout this paper. `smelli2.3.2` and `flavio2.3.3` have been updated to include the LEP-2 measurements as described in §4, as well as the updated combination of measurements of $B_{d,s} \rightarrow \mu^+\mu^-$ branching ratio measurements from Ref. [5].

We show the χ^2 improvement with respect to the SM in Fig. 4 as a function of the $U(1)_{Z'}$ electron charge divided by the muon charge, X_e/X_μ . As expected, the 23 measurements of LFU observables prefer $X_e/X_\mu = 1$ to lower values of the ratio that are substantially different from unity, where a χ^2 of 2 higher than in the SM is evident. The LEP-2 constraints pass through the origin, since $X_e = 0$ decouples the Z' from electron pairs, meaning that the tree-level predicted cross-sections are identical to those of the SM. An ‘LEP’ χ^2 contribution of up to 1 higher than the that of the SM is possible in the domain $X_e/X_\mu \in [-2, 2]$. On the other hand, the ‘quarks’ set of observables, which contains angular distributions of $B \rightarrow K^*\mu^+\mu^-$ decays and of branching ratios in different bins of di-muon invariant mass squared, enjoys a larger effect, improving χ^2 on the SM value by over 9 units in the domain taken. Adding all effects together in the ‘global’ fit, we see that in fact X_e/X_μ of around 1/2 is preferred. Both $X_e = 0$ and $X_\mu = X_e$ are with the 95% CL preferred region $-0.4 < X_e/X_\mu < 1.3$ (however, neither is within the 68% CL region).

The p -values associated with each fit, as well as the best-fit values of parameters, are displayed in the left-hand panel of Fig. 5. We see that the p -values of the three categories defined are all above the .05 level, indicating that no category has a terrible fit. The global p -values show a reasonable fit overall in the .15-.26 range throughout the domain of X_e/X_μ shown. However, we should bear in mind that the p -values have been ‘diluted’ by measure-

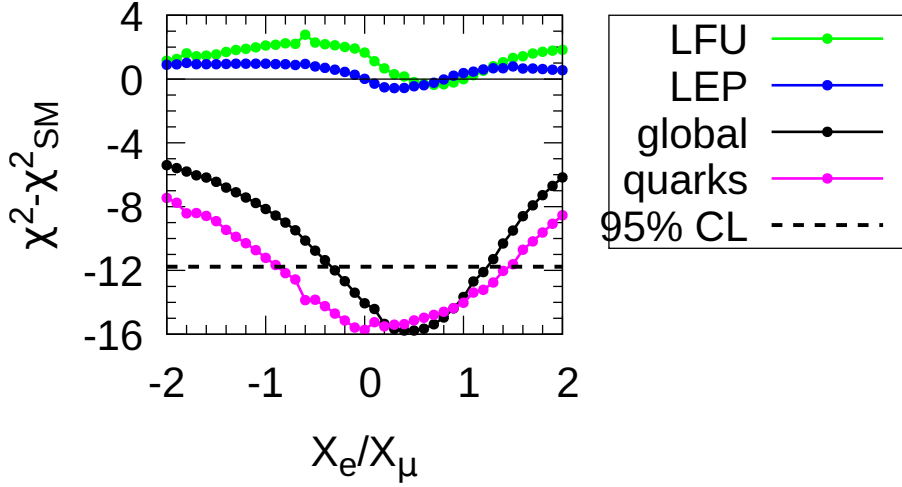


Figure 4. χ^2 improvement with respect to that of the SM as a function of electron charge divided by muon charge, X_e/X_μ . A negative value of $\chi^2 - \chi^2_{SM}$ indicates an *improvement* of the fit with respect to the SM whereas a positive value indicates a worse fit than the SM. ‘LFU’ contains 23 observables such as R_K and R_{K^*} , which test lepton flavour universality. ‘LEP’ contains the 148 $e^+e^- \rightarrow l^+l^-$ measurements discussed in §4. ‘quarks’ contains 224 other $b \rightarrow s\mu^+\mu^-$ measurements defined in flavio2.3.3. Under the hypothesis that the model line is correct, the region where the ‘global’ results are *below* the marked dashed line is within the 95% fit region.

ments included in some categories that have large errors (for example some of the Belle data in the ‘LFU’ category). We also see that the ‘quarks’ category is *not* fit perfectly; this could be due either to: the flavio2.3.3 predictions not having large enough theory errors ascribed to them, unaccounted for experimental systematic errors or that the set of models we have chosen is not the best one to describe the data in the category. In the right-hand panel of Fig. 5, we see some trends. The fact that $g_{Z'}$ falls towards the right-hand side and left-hand side of the plot can be seen as due to the fact that LEP constraints will prefer a smaller value of $g_{Z'}$ when $|X_e|$ is large, since then the Z' coupling to electrons is higher. When $g_{Z'}$ is smaller, θ_{sb} is higher. This is expected: since the non-zero tree-level new physics WET WC is constrained by the model to be

$$C_9^{(\mu)} = -\frac{X_\mu Q_3}{2} \frac{g_{Z'}^2}{M_{Z'}^2} \sin 2\theta_{sb}. \quad (5.1)$$

Requiring some particular fixed value of $C_9^{(\mu)} \neq 0$ to fit the quarks category, we see that $g_{Z'}/M_{Z'}$ would tend to move in the opposite direction as θ_{sb} .

The left-hand panel of Fig. 5 confirms that out of our set, globally, $X_e/X_\mu \approx 1/2$ provides a close-to-optimal fit to the experimental measurements included. The optimal model at this

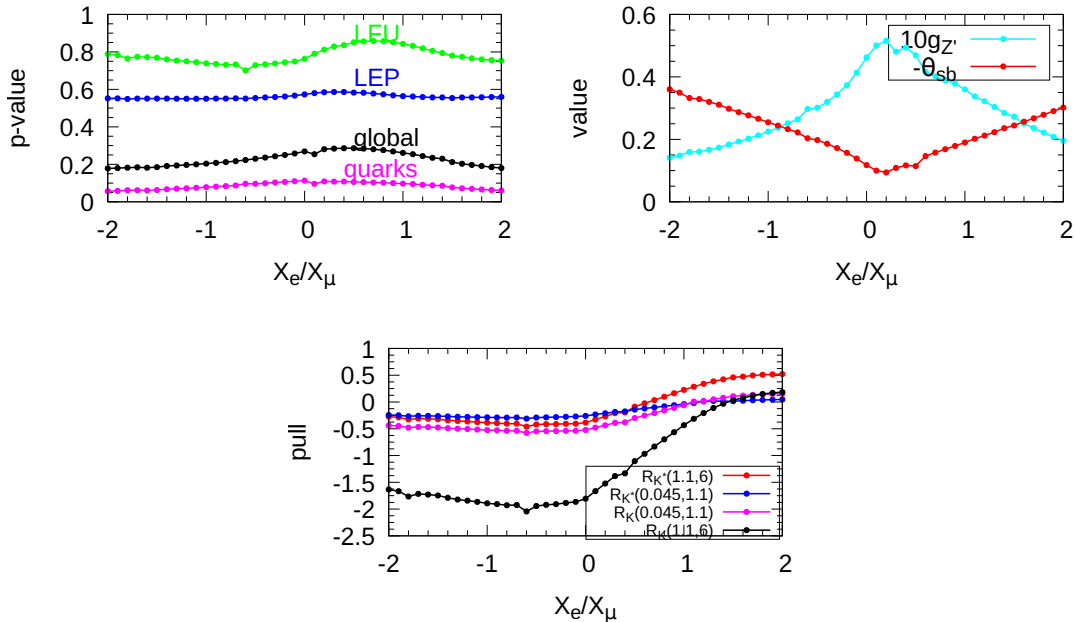


Figure 5. (left panel) p -values, (right panel) best-fit parameters and (bottom panel) 2022 LHCb LFU measurements associated with each model, as a function of X_e/X_μ , for $M_{Z'} = 3$ TeV. In the left panel, ‘LFU’ contains 23 observables (including the aforementioned 2022 LHCb LFU measurements) such as R_K and R_{K^*} , which test lepton flavour universality. ‘LEP’ contains the 148 $e^+e^- \rightarrow l^+l^-$ measurements discussed in §4. ‘quarks’ contains 224 other $b \rightarrow s\mu^+\mu^-$ measurements defined in flavio2.3.3. In the bottom panel, the legend displays the domain of invariant mass squared in GeV^2 in parenthesis and ‘pull’ is defined as $(p - e)/\sigma$, where p is the theoretical prediction of the best-fit point of the $U(1)_X$ model, e is the experimental central value and σ is the experimental uncertainty, ignoring correlations with other observables.

value of the ratio corresponds to fermionic charges of $3B_3 - 5L_e - 10L_\mu + 12L_\tau$. Some may feel that, aesthetically, some of the charges in this assignment are rather large. This suggests that we investigate a different model in our set with the same ratio of X_e/X_μ but with smaller X_μ . By adjusting $g_{Z'}$, we may expect the fit then to reach a similar $\chi^2 - \chi_{SM}^2$ for the LEP observables. We also expect that θ_{sb} will then change to keep the value of (5.1) invariant. There should be only small corrections to this overall χ^2 -invariant picture from the different gauge coupling affecting the renormalisation between $M_{Z'}$ and M_Z . One charge assignment with $X_e/X_\mu = 1/2$ which is anomaly-free is $3B_3 - L_e - 2L_\mu$. We shall investigate this model in more detail now.

5.1 $3B_3 - L_e - 2L_\mu$

Here, we perform a new fit to the $3B_3 - L_e - 2L_\mu$ model; the result is displayed in Table 3. We see that the overall fit is of an acceptable quality, with a p -value of .27. The higher invariant

	$\chi^2 - \chi_{SM}^2$	p -value	measurement	pull
LFU	-0.2	.81	$R_{K^*}(0.045, 1.1)$	-0.1
LEP	-0.4	.58	$R_{K^*}(1.1, 6)$	-0.1
quarks	-14.6	.10	$R_K(0.045, 1.1)$	-0.3
global	-15.3	.27	$R_K(1.1, 6)$	-1.1

Table 3. Quality-of-fit for the $3B_3 - L_e - 2L_\mu$ Z' model and the pulls of the 2022 LHCb LFU measurements. The numbers in parathesis refer to the end-points of the domain of the relevant bin of di-lepton invariant mass, in units of GeV^2 . For $M_{Z'} = 3 \text{ TeV}$, the best-fit parameters are $g_{Z'} = 0.222$, $\theta_{sb} = -0.0263$.

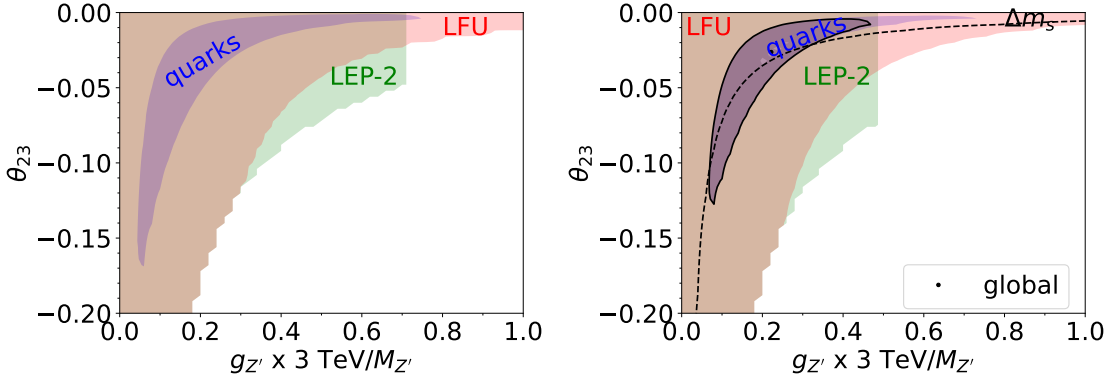


Figure 6. Parameter space of the $3B_3 - L_e - 2L_\mu$ model: (left) compatibility of different sets of observables and (right) constraints. ‘LFU’ contains 23 observables (including the aforementioned 2022 LHCb LFU measurements) such as R_K and R_{K^*} , which test lepton flavour universality. ‘LEP-2’ contains the 148 $e^+e^- \rightarrow l^+l^-$ measurements discussed in §4. ‘quarks’ contains 224 other $b \rightarrow s\mu^+\mu^-$ measurements defined in `flavio2.3.3`. In the left-hand panel, the coloured regions show where the p -value of each labelled constraint is greater than 0.05. In the right-hand panel, the coloured regions are the 95% confidence limit (CL) *allowed* regions defined by $\chi^2 - \chi^2(\text{min}) = 5.99$ [43] as shown by reference to the legend for the category of observable. The black line encloses the 95% CL global region and the black dot gives the locus of the best-fit point. The region above the dashed line is compatible with the $B_s - \overline{B}_s$ mixing constraint at the 95% CL (note that this measurement is one of those from the ‘quarks’ set).

mass-squared bin of R_K is compatible with its experimental value (the pull is 1.1σ), whereas the others are all very well fit. The $B_3 - L_e - 2L_\mu$ model has a χ^2 improvement of 15.3 as compared to the SM, for two additional fitted parameters. The p -value of the SM being as statistically as good a fit to the data⁵ as the $B_3 - L_e - 2L_\mu$ model is .0005.

We display the parameter space of the model in Fig. 6. One should interpret the left-

⁵The SM is equivalent to the parameter choice $g_{Z'} = 0$, $\theta_{sb} = 0$ of the $B_3 - L_e - 2L_\mu$ model under suitable caveats; therefore we use the optimal likelihood ratio test for two degrees of freedom to calculate the p -value.

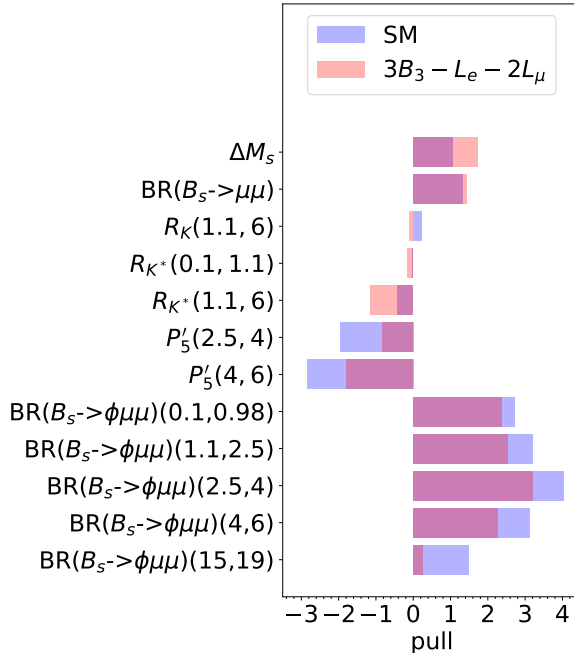


Figure 7. Various pulls of interest for the SM and the best-fit point of the $3B_3 - L_e - 2L_\mu$ model. Pull is defined as theory prediction minus the experimental central value divided by uncertainty. Correlation between observables is neglected in the calculation of the pull.

hand panel as testing the joint compatibility of measurements between different categories of observable in the model. We see, since the regions of acceptable fit (defined here to be p -value greater than .05) overlap, there is parameter space where each constraint is compatible with all of the measurements. The right-hand panel should be interpreted as parameter constraints upon the model, *assuming that the $3B_3 - L_e - 2L_\mu$ model hypothesis is correct*. Here, we see that the constraints from the ‘quarks’ category of observable is more-or-less compatible with the LFU constraints. The LEP-2 constraints cut off the global fit contour at the top-right hand side, for larger $g_{Z'}/M_{Z'}$. The $B_s - \bar{B}_s$ mixing constraint cuts off the global-fit region at the lower left-hand side. A curved region at the bottom right-hand side of the plot has too large flavour changing effects in general for `flavio2.3.3` to return a numerical answer, which explains why some of the constraints (notably from LEP-2) are bounded there. Such regions are expected to be highly ruled out by flavour measurements anyway.

We show the pulls of some observables of interest in Fig. 7. We see that although the $3B_3 - L_e - 2L_\mu$ model fits $B_s - \bar{B}_s$ mixing (as measured by Δm_s), $BR(B_s \rightarrow \mu^+\mu^-)$ and $R_{K^*}(1.1, 6)$ less well than the SM, it ameliorates the fit to more of the other observables. Various bins of $BR(B_s \rightarrow \phi\mu^+\mu^-)$, whilst fitting *better* than in the SM, are still far from optimal (the egregious one being 3σ between 2.5 and 4 GeV² in di-muon invariant mass squared). This goes some way to confirming the assertion in the discussion of Fig. 5 that the

fit to the ‘quarks’ category of observable, although acceptable, is far from perfect.

6 Conclusion

We have critically re-examined Z' models that can significantly ameliorate the $b \rightarrow s\mu^+\mu^-$ anomalies in global fits. The recent re-analysis of the R_K and R_{K^*} observables by LHCb implies that, if the $b \rightarrow s\mu^+\mu^-$ anomalies are due to beyond the SM effects, there may well also be beyond the SM effects in $b \rightarrow se^+e^-$. One obvious model is a TeV-scale Z' boson that couples dominantly to third family quarks, to $s\bar{b}$ and $b\bar{s}$ through weak mixing effects, to di-muon pairs and to di-electron pairs in addition. We identified a one-rational-parameter family of models in which, in the first two family charged-lepton sector, interpolates between a Z' only coupling to di-muon pairs and a Z' which couples to di-electron pairs and to di-muon pairs with equal strength. Here, the coupling strength is directly proportional to the $U(1)_{Z'}$ charge of the leptonic field in question. By coupling a Z' to di-electron pairs, one obtains constraints from LEP-2, which measured scattering of e^+e^- to di-lepton pairs and which viewed no significant deviations from SM predictions.

One hopefully useful side-product of the present paper was to re-calculate the predicted deviations resulting from relevant dimension-6 SMEFT operators. A previous presentation in the literature [38] has thus received an independent check. Our calculation is presented in a more complete form than Ref. [38], which guarantees that the resulting predicted LEP-2 cross-sections are positive even in extreme parts of parameter space. The calculations in the more complete form have been programmed into `smelli2.3.2` and `flavio2.3.3`, and are thus publicly available for use. Other experimental data such as electroweak precision observables, can be varied (or indeed re-fit) and the LEP-2 constraints will change accordingly in the calculation.

One particular model, $3B_3 - L_e - L_\mu - L_\tau$, was already examined in Ref. [39] (using the numerical results from a fit to old data) where it was found that there is no parameter region where each experimental constraint is satisfied to 1σ . We think this to be overly restrictive, and prefer a global fit strategy. By widening the model space to allow different electron and muon $U(1)_X$ charges, we also see how much the preference is for an equal coupling to di-electron pairs and di-muon pairs, as compared to some other ratio between the two. This main information is displayed in Fig. 4. From the figure, it appears that zero coupling of the Z' boson to di-electron pairs is roughly as good a fit as an equal coupling to di-muon pairs (which is a better fit by only 0.7 units of χ^2), globally. But we also see that a Z' which couples to di-electron pairs with about half the strength with which it couples to di-muon pairs is a close-to-optimal global fit, at least along a particular line in the space of rational charges. Thus, we are led to propose the $3B_3 - L_e - 2L_\mu$ model; its properties as regards flavour changing variables are investigated in §5.1. Here, Fig. 5 shows a sub-optimal fit to some observables in the ‘quark’ category of observable, even if the fit to the category as a whole is acceptable. Further lepton-flavour universal corrections to C_9 WCs coming from non-perturbative corrections may perhaps potentially ameliorate these.

Acknowledgements

This work was partially supported by STFC HEP Consolidated grant ST/T000694/1. We thank the Cambridge Pheno Working Group for discussions and P Stangl for helpful advice on the calculation of the LEP2 constraints and their insertion into the `flavio` and `smelli` computer programs. We thank CERN for hospitality extended while this work was carried out.

References

- [1] **ATLAS** Collaboration, M. Aaboud *et. al.*, *Study of the rare decays of B_s^0 and B^0 mesons into muon pairs using data collected during 2015 and 2016 with the ATLAS detector*, *JHEP* **04** (2019) 098 [[1812.03017](#)].
- [2] **CMS** Collaboration, *Measurement of $B_s^0 \rightarrow \mu^+ \mu^-$ decay properties and search for the $B^0 \rightarrow \mu \mu$ decay in proton-proton collisions at $\sqrt{s} = 13$ TeV*, .
- [3] **LHCb** Collaboration, R. Aaij *et. al.*, *Measurement of the $B_s^0 \rightarrow \mu^+ \mu^-$ branching fraction and effective lifetime and search for $B^0 \rightarrow \mu^+ \mu^-$ decays*, *Phys. Rev. Lett.* **118** (2017), no. 19 191801 [[1703.05747](#)].
- [4] **CMS** Collaboration, *Measurement of $B_s^0 \rightarrow \mu^+ \mu^-$ decay properties and search for the $B^0 \rightarrow \mu \mu$ decay in proton-proton collisions at $\sqrt{s} = 13$ TeV*, .
- [5] B. Allanach and J. Davighi, *The Rumble in the Meson: a leptoquark versus a Z' to fit $b \rightarrow s \mu^+ \mu^-$ anomalies including 2022 LHCb $R_{K^{(*)}}$ measurements*, *JHEP* **04** (2023) 033 [[2211.11766](#)].
- [6] **LHCb** Collaboration, R. Aaij *et. al.*, *Angular analysis and differential branching fraction of the decay $B_s^0 \rightarrow \phi \mu^+ \mu^-$* , *JHEP* **09** (2015) 179 [[1506.08777](#)].
- [7] **CDF** Collaboration, *Precise Measurements of Exclusive $b \rightarrow s \mu^+ \mu^-$ Decay Amplitudes Using the Full CDF Data Set*, .
- [8] **LHCb** Collaboration, R. Aaij *et. al.*, *Measurement of Form-Factor-Independent Observables in the Decay $B^0 \rightarrow K^{*0} \mu^+ \mu^-$* , *Phys. Rev. Lett.* **111** (2013) 191801 [[1308.1707](#)].
- [9] **LHCb** Collaboration, R. Aaij *et. al.*, *Angular analysis of the $B^0 \rightarrow K^{*0} \mu^+ \mu^-$ decay using 3 fb^{-1} of integrated luminosity*, *JHEP* **02** (2016) 104 [[1512.04442](#)].
- [10] **ATLAS** Collaboration, M. Aaboud *et. al.*, *Angular analysis of $B_d^0 \rightarrow K^{*0} \mu^+ \mu^-$ decays in pp collisions at $\sqrt{s} = 8$ TeV with the ATLAS detector*, *JHEP* **10** (2018) 047 [[1805.04000](#)].
- [11] **CMS** Collaboration, A. M. Sirunyan *et. al.*, *Measurement of angular parameters from the decay $B^0 \rightarrow K^{*0} \mu^+ \mu^-$ in proton-proton collisions at $\sqrt{s} = 8$ TeV*, *Phys. Lett. B* **781** (2018) 517–541 [[1710.02846](#)].
- [12] **CMS** Collaboration, V. Khachatryan *et. al.*, *Angular analysis of the decay $B^0 \rightarrow K^{*0} \mu^+ \mu^-$ from pp collisions at $\sqrt{s} = 8$ TeV*, *Phys. Lett. B* **753** (2016) 424–448 [[1507.08126](#)].
- [13] C. Bobeth, M. Chrzaszcz, D. van Dyk and J. Virto, *Long-distance effects in $B \rightarrow K^{*} \ell \ell$ from analyticity*, *Eur. Phys. J. C* **78** (2018), no. 6 451 [[1707.07305](#)].

- [14] **HPQCD** Collaboration, W. G. Parrott, C. Bouchard and C. T. H. Davies, *Standard Model predictions for $B \rightarrow K\ell^+\ell^-$, $B \rightarrow K\ell^1\ell^2+$ and $B \rightarrow K\nu\nu^-$ using form factors from $N_f=2+1+1$ lattice QCD*, *Phys. Rev. D* **107** (2023), no. 1 014511 [[2207.13371](#)].
- [15] M. Algueró, A. Biswas, B. Capdevila, S. Descotes-Genon, J. Matias and M. Novoa-Brunet, *To $(b)e$ or not to $(b)e$: No electrons at LHCb*, [2304.07330](#).
- [16] Q. Wen and F. Xu, *The Global Fits of New Physics in $b \rightarrow s$ after $R_{K^{(*)}}$ 2022 Release*, [2305.19038](#).
- [17] J. Aebischer, J. Kumar, P. Stangl and D. M. Straub, *A Global Likelihood for Precision Constraints and Flavour Anomalies*, *Eur. Phys. J. C* **79** (2019), no. 6 509 [[1810.07698](#)].
- [18] N. Gubernari, M. Reboud, D. van Dyk and J. Virto, *Improved theory predictions and global analysis of exclusive $b \rightarrow s\mu^+\mu^-$ processes*, *JHEP* **09** (2022) 133 [[2206.03797](#)].
- [19] N. Gubernari, M. Reboud, D. van Dyk and J. Virto, *Dispersive Analysis of $B \rightarrow K^{(*)}$ and $B_s \rightarrow \phi$ Form Factors*, [2305.06301](#).
- [20] M. Ciuchini, M. Fedele, E. Franco, A. Paul, L. Silvestrini and M. Valli, *Constraints on lepton universality violation from rare B decays*, *Phys. Rev. D* **107** (2023), no. 5 055036 [[2212.10516](#)].
- [21] A. J. Buras and E. Venturini, *The exclusive vision of rare K and B decays and of the quark mixing in the standard model*, *Eur. Phys. J. C* **82** (2022), no. 7 615 [[2203.11960](#)].
- [22] A. J. Buras, *Standard Model predictions for rare K and B decays without new physics infection*, *Eur. Phys. J. C* **83** (2023), no. 1 66 [[2209.03968](#)].
- [23] **LHCb** Collaboration, *Test of lepton universality in $b \rightarrow s\ell^+\ell^-$ decays*, [2212.09152](#).
- [24] **LHCb** Collaboration, R. Aaij *et. al.*, *Tests of lepton universality using $B^0 \rightarrow K_S^0\ell^+\ell^-$ and $B^+ \rightarrow K^{*+}\ell^+\ell^-$ decays*, *Phys. Rev. Lett.* **128** (2022), no. 19 191802 [[2110.09501](#)].
- [25] B. Grzadkowski, M. Iskrzynski, M. Misiak and J. Rosiek, *Dimension-Six Terms in the Standard Model Lagrangian*, *JHEP* **10** (2010) 085 [[1008.4884](#)].
- [26] P. Stangl, *smelli – the SMEFT Likelihood*, *PoS TOOLS2020* (2021) 035 [[2012.12211](#)].
- [27] R. J. Barlow, *Statistics: A Guide to the Use of Statistical Methods in the Physical Sciences*. Wiley, 1989.
- [28] B. C. Allanach, *$U(1)_{B_3-L_2}$ explanation of the neutral current B -anomalies*, *Eur. Phys. J. C* **81** (2021), no. 1 56 [[2009.02197](#)]. [Erratum: *Eur.Phys.J.C* 81, 321 (2021)].
- [29] B. C. Allanach and J. Davighi, *Third family hypercharge model for $R_{K^{(*)}}$ and aspects of the fermion mass problem*, *JHEP* **12** (2018) 075 [[1809.01158](#)].
- [30] B. C. Allanach and J. Davighi, *Naturalising the third family hypercharge model for neutral current B -anomalies*, *Eur. Phys. J. C* **79** (2019), no. 11 908 [[1905.10327](#)].
- [31] B. Allanach and J. Davighi, *M_W helps select Z' models for $b \rightarrow s\ell\ell$ anomalies*, *Eur. Phys. J. C* **82** (2022), no. 8 745 [[2205.12252](#)].
- [32] B. C. Allanach, J. Davighi and S. Melville, *An Anomaly-free Atlas: charting the space of flavour-dependent gauged $U(1)$ extensions of the Standard Model*, *JHEP* **02** (2019) 082 [[1812.04602](#)]. [Erratum: *JHEP* 08, 064 (2019)].

- [33] B. C. Allanach, B. Gripaios and J. Tooby-Smith, *Anomaly cancellation with an extra gauge boson*, *Phys. Rev. Lett.* **125** (2020), no. 16 161601 [[2006.03588](#)].
- [34] C. Froggatt and H. Nielsen, *Hierarchy of quark masses, cabibbo angles and cp violation*, *Nuclear Physics B* **147** (1979), no. 3 277–298.
- [35] B. Allanach and E. Loisa, *Flavonstrahlung in the $B_3 - L_2 Z'$ model at current and future colliders*, *JHEP* **03** (2023) 253 [[2212.07440](#)].
- [36] **Particle Data Group** Collaboration, R. L. Workman *et. al.*, *Review of Particle Physics*, *PTEP* **2022** (2022) 083C01.
- [37] D. M. Straub, *flavio: a Python package for flavour and precision phenomenology in the Standard Model and beyond*, [1810.08132](#).
- [38] A. Falkowski and K. Mimouni, *Model independent constraints on four-lepton operators*, *JHEP* **02** (2016) 086 [[1511.07434](#)].
- [39] A. Greljo, J. Salko, A. Smolkovič and P. Stangl, *Rare b decays meet high-mass Drell-Yan*, *JHEP* **05** (2023) 087 [[2212.10497](#)].
- [40] I. Brivio and M. Trott, *The Standard Model as an Effective Field Theory*, *Phys. Rept.* **793** (2019) 1–98 [[1706.08945](#)].
- [41] **ALEPH, DELPHI, L3, OPAL, LEP Electroweak** Collaboration, S. Schael *et. al.*, *Electroweak Measurements in Electron-Positron Collisions at W-Boson-Pair Energies at LEP*, *Phys. Rept.* **532** (2013) 119–244 [[1302.3415](#)].
- [42] J. Aebischer, J. Kumar and D. M. Straub, *Wilson: a Python package for the running and matching of Wilson coefficients above and below the electroweak scale*, *Eur. Phys. J. C* **78** (2018), no. 12 1026 [[1804.05033](#)].
- [43] F. James and M. Winkler, *MINUIT User's Guide*, .